A Bayesian Hierarchical Space-Time Model Applied to High-Resolution Hindcast Data of Significant Wave Height

Erik Vanem

Det Norske Veritas, DNV R&I

Veritasveien 1, 1322 Høvik, Norway

E-mail: Erik.Vanem@dnv.com

1. Introduction

The models presented in this paper are stochastic models in space and time that aim at describing the distribution of significant wave height in space and time. They are fitted to data for an area in the North Atlantic Ocean and estimate the complex spatio-temporal dependence structure at various scales inherent in the data. The models were developed as part of a PhD study at the University of Oslo (Vanem 2012, 2013) and have previously been fitted to corrected ERA-40 data for the North Atlantic (Caires and Swail 2004; Sterl and Caires 2005).

In recent years, it has become increasingly evident that the globe is experiencing a change in climate, mostly due to human activities and emission of greenhouse gases. In this context, it becomes important to understand how such changes may impact the ocean wave climate and subsequently how this may impact the environmental loads on marine structures (Bitner-Gregersen et al. 2012; DNV 2010, 2011; Vanem and Bitner-Gregersen 2012). Hence, the models presented in this report include a component for describing long-term trends in the data for significant wave height. Such trends may then be extrapolated to give indications of possible future trends in the wave climate. Previously, model alternatives with linear and quadratic trend functions (Vanem et al. 2012a), with a log-transform of the data (Vanem et al. 2012b) and with regression on atmospheric CO_2 levels (Vanem et al. 2013) have been developed and applied to the C-ERA-40 data of significant wave height. The various model alternatives all identified increasing trends in the significant wave height data over the area in the North Atlantic, a finding that has also been substantiated by various time-series trend analyses techniques as presented in Vanem and Walker (2012). The same modelling framework has also been applied to wind speed data over the same area, as reported in Vanem and Breivik (2013), but failed to identify any significant trends for the windiness. Presumably, this may indicate that the observed increase in waviness is due to increased swell.

In this paper, the Bayesian hierarchical space-time model will be applied to NORA10 data (Reistad et al. 2011, 2007) of significant wave height for an overlapping area of the North Atlantic. The Nora10 is a regional hindcast obtained by dynamical downscaling of the ERA-40 data, producing 3-hourly wave fields at 10-11 km grid spacing. The atmospheric forcing is obtained with the 10-km resolution HIRLAM10 model (Undén et al. 2002). Compared to the C-ERA-40 data, with a spatial resolution of 1.5 x 1.5 degrees (corresponding to about 167 km grid spacing in lateral direction and between 76 and 105 km grid spacing in longitudinal direction (Vanem et al. 2011)), the NORA10 data has a much higher spatial resolution and is believed to be more accurate. It has also been reported that the NORA10 data yields significantly higher return values compared to the ERA-40 data (Breivik et al. 2013). 100-year return value estimates for the NORA10 data of significant wave height were presented in Aarnes et al. (2012).

By applying the same model on the NORA10 data that has previously been applied to C-ERA-40 data, the results may be compared and the effect of the increased spatial resolution can be evaluated. Furthermore, it is interesting to investigate whether similar long-term temporal trends are present in the NORA10 data and to provide estimates of these trends.

2. Data and Area Description

The study presented in this paper has analysed the NORA10 significant wave height data for a selected area in the North Atlantic Ocean. In the following, the selected area and the data for significant wave height will be described. The models have used regression on CO_2 levels in the atmosphere in order to estimate long-term trends, and both historical CO_2 data and future projections are needed, for fitting the model and for making projections of the wave climate, respectively.

North-Atlantic area selected for the analysis

The area selected for this analysis is an area in the North Atlantic Ocean that is partly overlapping with the area that was selected for analysis with the C-ERA-40 data.

TABLE 1. Coordinates of the corners of the NORA10 area; (Degrees North, Degrees East)

Corner	West	East
North	(62.59, 16.37)	(60.39, 6.97)
South	(57.9, 19.87)	(55.99, 11.5)

It has been chosen so that the area is some distance away from the boundary of the NORA10 model domain so that possible edge-effects are minimized. In Fig. 1, the area that has previously been investigated based on C-ERA-40 data is shown together with the new area analysed by the NORA10 data.

As can be seen from Fig. 1, the area for the C-ERA-40 data is much larger than the area for the NORA10 data. However, due to the much higher resolution of the NORA10 data, the latter area contains a much larger number of grid points. The green area in the figure contains 9 x 17 = 153 C-ERA-40 data points whereas the smaller blue area contains 51 x 51 = 2601 NORA10 data points. Thus, the analysed NORA10 data contain 17 times more spatial data-points than the C-ERA-40 data.

The C-ERA-40 data lie on a cylindrical grid, between 51 and 63 degrees north and 12 and 36 degrees west, with grid points 1.5 degrees apart in both directions. Hence, the geographical distance between data points differs with latitude, with about 167 km grid spacing in lateral direction and between 76 (northernmost) and 105 (southernmost) km grid spacing in longitudinal direction (Vanem et al. 2011). The NORA10 data, on the other hand, lies on a rotated spherical equidistant grid, with a spatial separation of 10 km between grid points in both directions. This means that the grid points do not correspond to integer longitude and latitude, but the geographical distance between neighbouring points is constant throughout the grid. The coordinates of the four corners of the NORA10 area are given in Table 1.

Even though the area for the NORA10 data is much smaller than the area previously analysed with C-ERA-40 data, the much higher resolution means that the amount of spatial data is significantly higher. This slows down the computation and it was decided to run five sets of simulations. First, the NORA10 area is divided into four quarters and simulations are run separately for each quarter-area with half the spatial resolution, corresponding to four areas with 13 x 13 = 169 grid points. Subsequently, simulations are run on the whole area with reduced spatial resolution, i.e. using every fourth data-point to obtain a grid with 40 km separation between the grid points. The results for the complete area can then be compared with the results pertaining to each of the quarter-areas. The coordinates of the corners in each of the quarter-areas are given in Table 2, and the quarter-areas are indicated in Fig. 1.

TABLE 2. Coordinates of the edges of the quarter-areas; (∘N, degE)

Quarter-area	Coordinates of the edges	
Q1	(60.17, 18.34)	(59.26, 13.93)
	(57.90, 19.87)	(57.06, 15.74)
Q2	**(62.59, 16.37)**	(61.62, 11.69)
	(60.35, 18.18)	(59.45, 13.77)
Q3	(59.18, 13.58)	(58.12, 9.47)
	(56.99, 15.40)	**(55.99, 11.50)**
Q4	(61.53, 11.32)	**(60.39, 6.97)**
	(59.36, 13.41)	(58.30, 9.29)

NORA10 data for significant wave height

The NORA10 data stem from a combined high-resolution atmospheric downscaling and wave hindcast based on the ERA-40 reanalysis over the north-east Atlantic (Reistad et al. 2011). Atmospheric forcing is obtained from the 10-km High-Resolution Limited Area Model (HIRLAM10) (Undén et al. 2002) and wave simulations are made by a modified version of the WAM cycle 4 model (Komen et al. 1994), run on the same grid as HIRLAM10 (WAM10). This is nested inside a WAM model at 50-km resolution (WAM50) forced by ERA-40 wind fields covering the most of the North Atlantic to account for swell intrusion from the North Atlantic. South Atlantic swell intrusion is neglected.

The NORA10 data set for significant wave height contains 3-hourly wave fields with a spatial resolution of 10-11 km and covers an area in the north-east Atlantic including the North Sea, the Norwegian Sea and the Barents Sea. The complete NORA10 domain is illustrated in Fig. 2, which also indicates the area selected for study in this work.

Initially, NORA10 covered the time period September 1957 - August 2002, but the NORA10 data set is continually being extended using operational analyses from the ECMWF (European Centre for Medium-Range Weather Forecasts) as boundary and initial conditions (Aarnes et al. 2012). Hence, the NORA10 data set analysed in this paper spans the period January 1958 - December 2012, and the actual analysis considers data from January 1959 to December 2012. Data for the year 1958 were excluded from the analysis because CO_2 data were not available before March 1958. For the purpose of fitting the Bayesian hierarchical model, monthly maximum data have been used, and the monthly maxima at each spatial location have been extracted for each month of the 55-year period 1958 - 2012. Hence, time-series of 660 data points in time for each of the

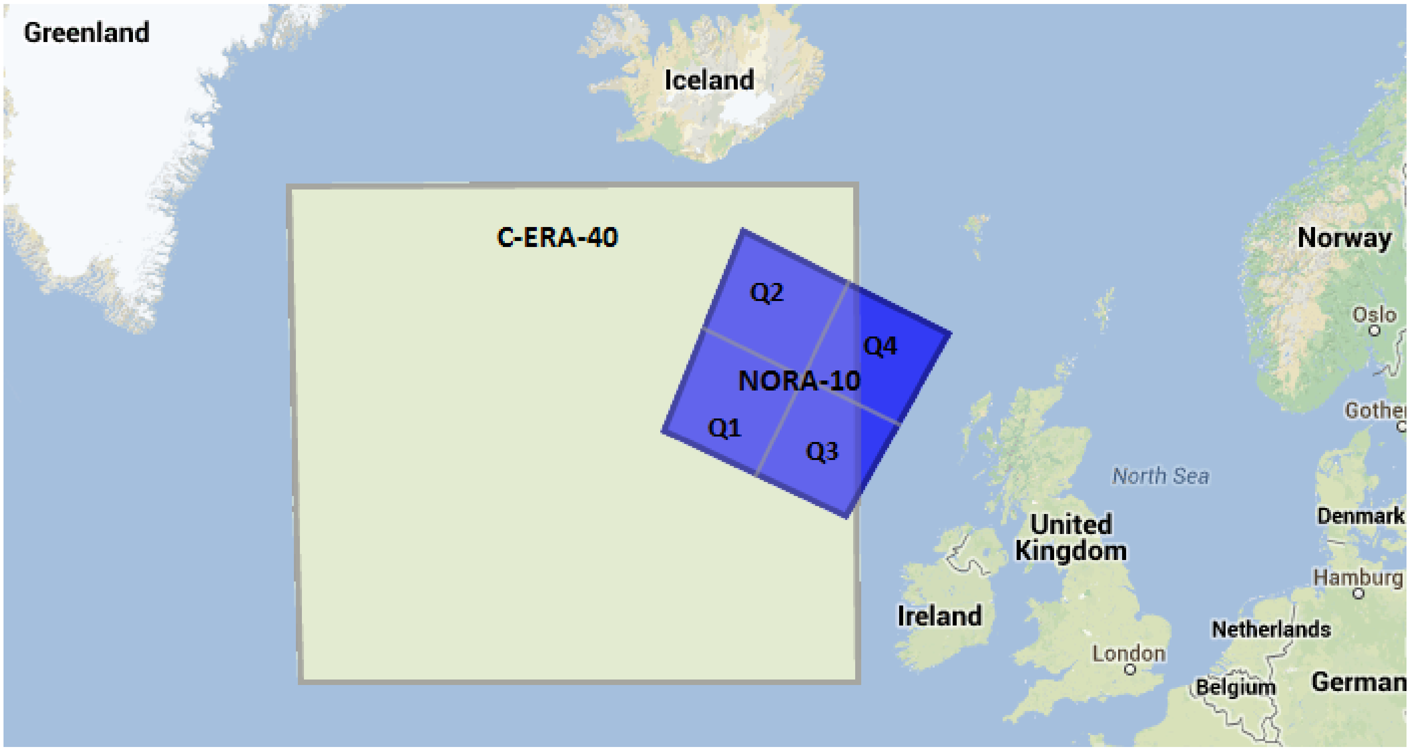

Fig. 1. Areas in the North Atlantic selected for study. The area analysed with C-ERA-40 data (green) and the area analysed with NORA10 data (blue)

2601 spatial grid points, totalling 1 716 660 data points in space and time, extracted from NORA10 form the basis for the analysis presented herein. However, due to time consuming simulations, the spatial resolution has been reduced before running the simulations, as outlined above.

Comparison with in situ measurements and satellite observations is reported in Reistad et al. (2011) and reveals that the NORA10 data yields a significant improvement compared to the ERA-40 data. For example, the ERA-40 data consistently underestimate the mean wave height, a bias that is not reproduced by the downscaling. Furthermore, root mean square errors are higher for the ERA-40 data compared to NORA10. Hence, it is assumed that the NORA10 represents a significant improvement compared to ERA-40 and that the NORA10 data are superior. In particular, it is well accepted that the upper percentiles of the significant wave height distribution are underestimated by ERA-40 and NORA10 yields significantly higher return values. Comparison of significant wave height from ERA-40 and the coarser WAM50 indicates a very close correlation

Initial data analysis

A brief initial data inspection reveals that the mean significant wave height in the dataset described above is 7.9 m (monthly maximum data). This is higher than for the C-ERA-40 data where the mean value was 7.5 m. The minimum value is 2.4 m and the maximum value is 21.7 m in the NORA10 data.

The average monthly maxima for individual months in the NORA10 data are given in Table 3. Included in the table are also the corresponding averages for the C-ERA-40 data for comparison (Vanem 2013), and it is interesting to observe that the monthly maxima from the NORA10 data are consistently higher than for the C-ERA-40 data; For each individual month the average monthly maximum over the data period is higher in the NORA10 data. Differences range from 0.24 m to as much as 1.91 m for the month of March. Overall, the average monthly maximum is 41 cm higher in the NORA10 data. The minimum and maximum values for individual months (monthly maximum for the NORA10 data) are also presented in Table 3.

The density of the monthly maximum data from the NORA10 is shown in Figure 3, where also the density for the monthly maximum data from C-ERA-40 is shown. It is seen that the densities are largely overlapping even though the NORA10 density seems to be slightly shifted towards higher values. This indicates that the NORA10 data generally has slightly higher values for the monthly maximum significant wave height, as expected.

Table 3. Average monthly maxima for individual months in the NORA10 data and comparison with C-ERA-40 data. Minimum and maximum monthly maximum significant wave height for individual months. (m)

	Jan	Feb	Mar	Apr	May	Jun	Jul	Aug	Sep	Oct	Nov	Dec	Overall
NORA10	10.6	10.0	9.09	7.30	6.23	5.27	4.95	5.33	7.60	8.75	9.40	10.2	7.89
C-ERA-40	9.87	8.91	7.18	5.89	5.89	5.03	4.42	5.04	6.96	8.21	8.69	9.79	7.48
Difference	0.73	1.09	1.91	1.41	0.34	0.24	0.53	0.29	0.64	0.54	0.71	0.41	0.41
Min	5.9	5.0	4.5	4.1	3.0	2.6	2.4	2.6	4.0	3.6	5.0	5.6	2.4
Max	21.7	17.4	16.3	13.0	13.0	10.0	10.2	11.5	14.5	15.0	18.7	18.5	21.7

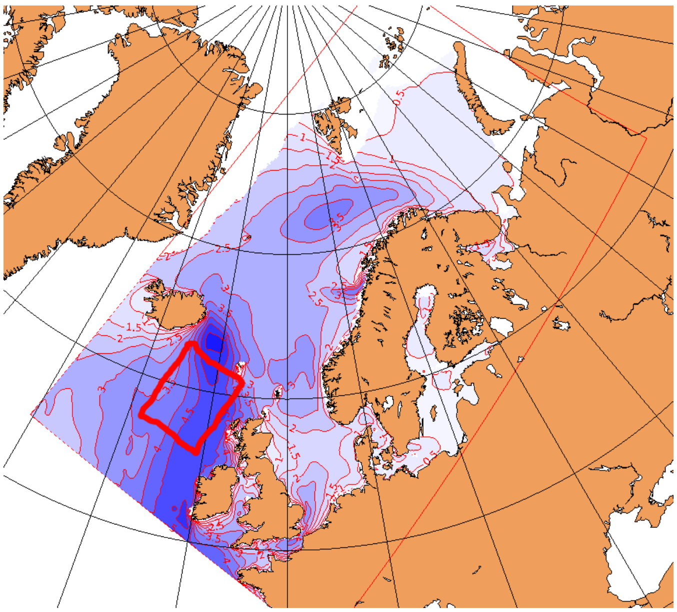

Fig. 2. The NORA10 model domain

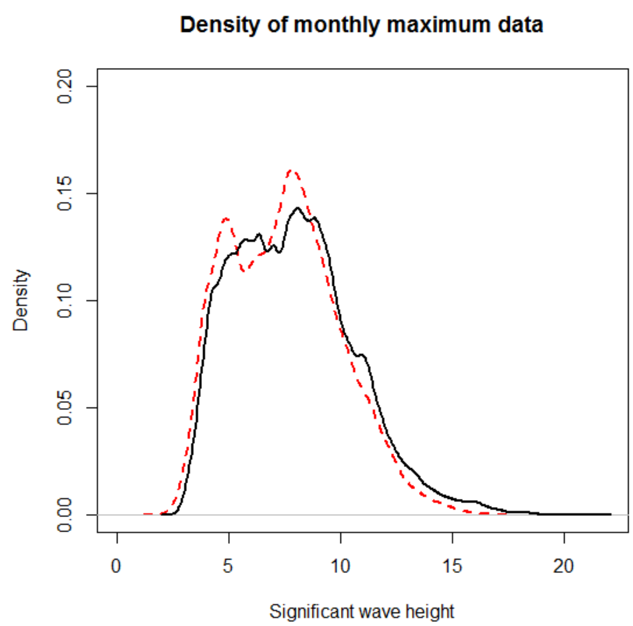

Fig. 3. The density of the NORA10 data for monthly maximum significant wave height (black line). For comparison, the density of the C-ERA-40 data is also shown (red dotted line)

A particular interest is in estimating possible long-term trends in the data. A crude approach could be to fit a straight line to time series of the data by least squares. In Fig. 4 such straight lines are fitted to time-series of spatial mean, spatial maxima and spatial minima of the NORA 10 data (a similar exercise was reported for the ERA-40 data in Vanem and Walker (2012)). The estimated intercepts and slopes of the fitted straight lines as well as the associated accumulated trends over the data period are presented in Table 4. This crude exercise suggests that there are increasing trends in the spatial min, mean and max time series, with highest trends for the spatial maxima at almost 70 cm over the data period. For the average, an estimated overall trend of about 29 cm is obtained in this way. However, the time series are quite noisy, and the p-values of the estimated trends are 0.398 (spatial min), 0.463 (spatial mean) and 0.0854 (spatial max), respectively.

Hence, even though the least square approach estimates an increasing trend in the data, the trends are not found to be statistically significant at 95% or 99% significance level. For the spatial maxima, the trend is statistically significant at the 90% level, but the spatial minima and mean fail to be significant at any reasonable significance level.

It is noted that when the same crude exercise of fitting a straight trend-line by least squares was made for the C-ERA-40 data, the estimated trends were found to be statistically significant at 99% level (p-values were not reported in Vanem and Walker (2012), but all were very small).

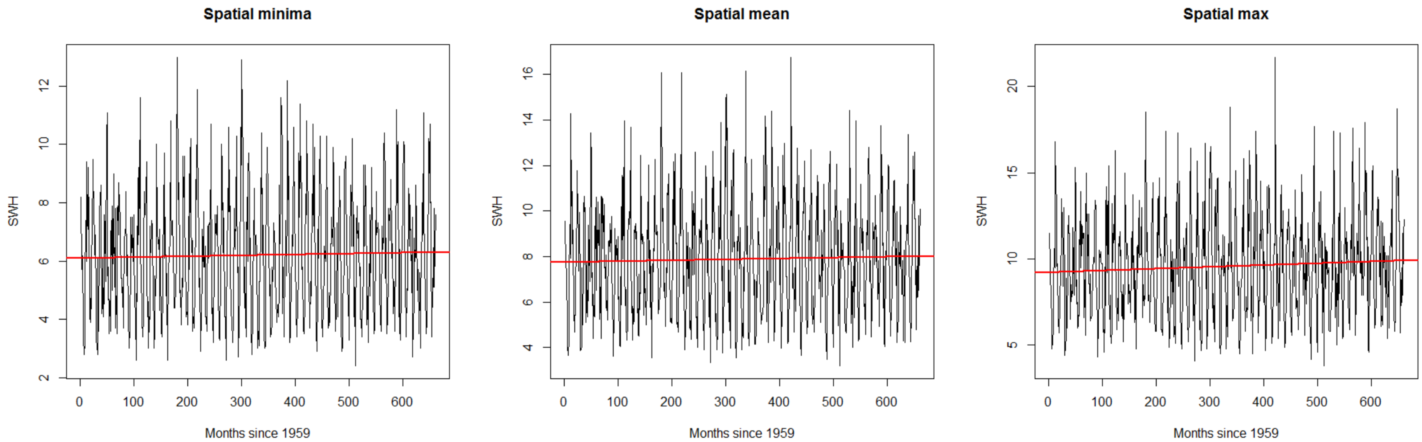

FIG. 4. Initial trend analysis: Fitting a straight line by least squares to time series of spatial minima (left), spatial averages (middle) and spatial maxima (right)

TABLE 4. Estimated parameters of straight lines fitted by least squares and corresponding trends

	Spatial Min	Spatial Mean	Spatial Max
Intercept	6.1058	7.7474	9.2130
Slope	0.0003138	0.0004393	0.001056
p-value of the slope	0.398	0.463	0.0854
Annual trend (cm)	0.3765	0.5272	1.268
Accumulated trend (cm)	20.71	28.99	69.72

CO_2 data

Concentrations of atmospheric CO_2 have been used as covariates for explaining possible long-term trends in the significant wave height data, and basically two sets of data have been exploited; historic data for model fitting and projections of future concentration levels for future predictions. The same CO_2 data as was used in the analysis of the ERA-40 data will be used, as described in Vanem et al. (2013), and a brief description will be repeated below.

HISTORIC DATA

For the purpose of this study, where the aim of introducing a regression component with CO_2 levels as covariates into the model is to identify long-term trends, it is deemed sufficient to use monthly data. Hence, monthly average CO_2 data from the Mauna Loa Observatory, Hawaii, which has the longest continuous record of direct atmospheric CO_2 measurements, have been used (Thoning et al. 1989). The data are on the format of number of molecules of carbon dioxide divided by the number of molecules of dry air multiplied by one million (parts per million = ppm), and data are available from March 1958 to present. The data set contains the monthly averages determined from daily averages, as well as interpolated monthly averages where missing data have been replaced by interpolated values. Finally, monthly trend values are given where the seasonal cycle has been removed and where linear interpolation has been used for missing months. For the purpose of this study, the monthly trend time series will be used as covariates for the long term trend. The seasonal cycle in the monthly maximum significant wave height is accounted for in a separate seasonal component in the Bayesian hierarchical model. The monthly trend CO_2 time series are shown in Fig. 5. It is noted that the CO_2 data for 1958 are not complete and therefore the analysis reported herein will start from January 1959.

It is also noted that the data stem from observations outside of the area in the North Atlantic which is the focus of this study. However, it is assumed that CO_2 is well mixed in the atmosphere, and that this does not introduce any notable bias in the monthly trend values. Hence this assumption is not regarded to be critical and should not influence the results of the analysis.

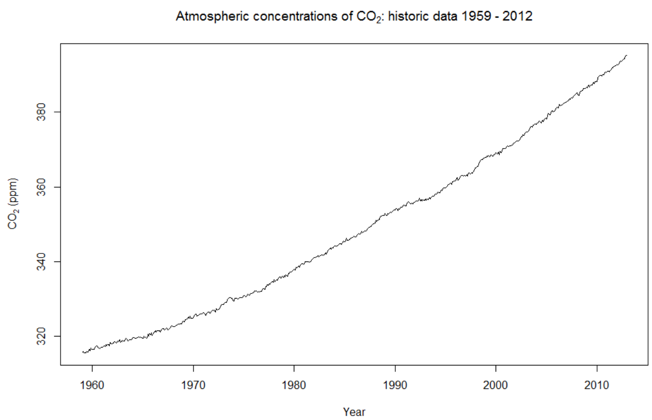

FIG. 5. Historic CO_2 concentrations in the atmosphere, 1959 - 2012

Future projections

In order to make projections of future wave climate, future projections of the covariates are needed and projections of the atmospheric concentration of CO_2 will be exploited. Future predictions are of course uncertain and different projections of CO_2 levels have been made based on different emission scenarios. Four scenarios are referred to as marker scenarios, supplemented with several illustrative scenarios. For the purpose of this study, projected emissions and concentrations presented by IPCC for the four marker scenarios (A1B, A2, B1 and B2), obtained from the ISAM carbon cycle Jain et al. (1995), have been considered. It is observed that the scenarios A2 and B1 correspond to the highest and lowest projected CO_2 levels respectively, and it is therefore assumed sufficient to employ these two in the modelling, as the other scenarios will fall between these. Scenario A2 might be an extreme scenario, but from a precautionary perspective it is important to include this in the analysis as this could be construed as a worst case scenario. The CO_2 projections data can also be found in appendix II of the IPCC (2001) report IPCC (2001).

The projected levels of atmospheric CO_2 concentrations are given for every 10 year towards 2100. For the purpose of this study, monthly averages are needed, and simple linear interpolation within each decade has been used in order to estimate monthly projections. The decadal projections are then assumed as the value for January of that year. In this way, monthly projections of CO_2 levels in the atmosphere from year 2013 until 2100 are obtained for use as covariates in the regression component of the stochastic model for significant wave height. The interpolated monthly projections are plotted in Fig. 6.

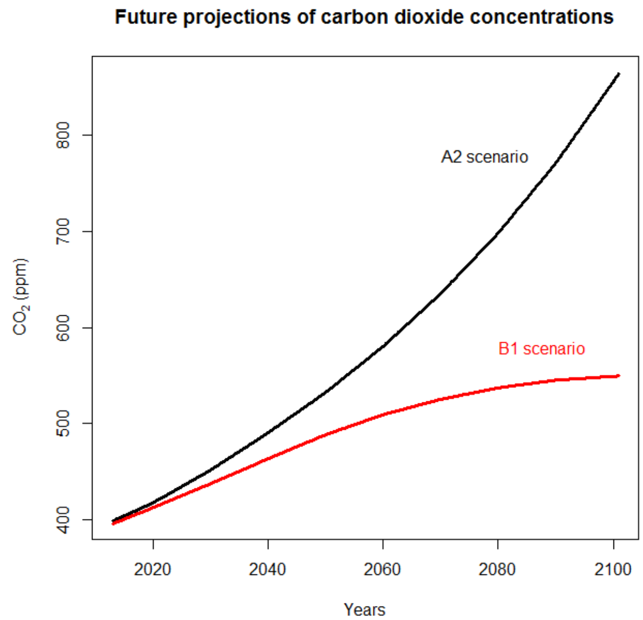

FIG. 6. Future projections of CO_2 concentrations in the atmosphere; A2 and B1 scenarios from 2013 - 2100

3. The Bayesian hierarchical space-time model

Various versions of the statistical model used in analysing the data have previously been presented in various papers, and will only be briefly presented in the following. The model used in this study is essentially the same as the one presented in Vanem et al. (2013), where regression on atmospheric CO_2 levels is included.

The spatio-temporal data are indexed by two indices; an index x to denote spatial location ($x = 1, 2, \ldots, X = 169$ in the simulations reported herein), and an index t to denote a point in time (i.e. months, $t = 1, 2, \ldots, T = 648$ for monthly maxima data in the simulations reported herein). The structure of the model will be outlined in the following. It is noted that all the stochastic terms introduced in the model are assumed mutually independent and independent in space and time, having a zero-mean Gaussian distribution with some random, but identical variance, i.e. with generic notation $\varepsilon_\beta \overset{i.i.d}{\sim} N(0, \sigma_\beta^2)$. It should be understood that the model is defined $\forall x \geq 1, t \geq 1$, as relevant for each component.

Model description

At the first level, the observations (monthly maximum significant wave height), Z at location x and time t, are modelled in the observation model as the latent variable H, corresponding to the underlying significant wave height process, and some random noise, ε_Z, which may be construed to include statistical measurement error:

$$Z(x,t) = H(x,t) + \varepsilon_z(x,t) \tag{1}$$

The underlying process for the significant wave height at location x and time t is modelled by the following state model, which is split into a time-independent component, $\mu(x)$, a space-time interaction component, $\theta(x,t)$, and spatially independent components $M(t)$ and $T(t)$ for seasonal and long-term trend contributions respectively, as shown in eq. (2). The long-term trend component is assumed spatially invariant and models the effect of climate change on the ocean wave climate.

$$H(x,t) = \mu(x) + \theta(x,t) + M(t) + T(t) \tag{2}$$

The time-independent spatial field is modelled as a first-order Markov Random Field (MRF), conditional on its nearest neighbours in all cardinal directions, and with different dependence parameters in lateral and longitudinal directions, as shown in eq. (3). Even though the data is on a rotated grid so that the data points do not strictly lie along north-south and east-west lines, the following notation has been used: $x^D =$ the location of the nearest grid point in direction D from x, where $D \in \{N,S,W,E\}$ and $N =$ "North", $S =$ "South", $W =$ "West" and $E =$ "East". Hence, for instance the point x^N should be construed to be the nearest grid point immediately to the north-east of x (see Fig. 1). The other directions are rotated in a similar way from the strictly north-south/east-west coordinate system. If x is at the border of the area, the value at the corresponding neighbouring grid point outside the area is taken to be zero, hence no particular measures are taken to correct for edge effects.

$$\begin{aligned}\mu(x) =& \mu_0(x) + a_\phi \left\{\mu(x^N) - \mu_0(x^N) + \mu(x^S) - \mu_0(x^S)\right\} \\ &+ a_\lambda \left\{\mu(x^W) - \mu_0(x^W) + \mu(x^E) - \mu_0(x^E)\right\} + \varepsilon_\mu(x)\end{aligned} \tag{3}$$

a_ϕ and a_λ are spatial dependence parameters in the main directions of the grid, i.e. lateral (northeast - southwest direction as from areas $Q1 \leftrightarrow Q2$ in Fig. 1) and longitudinal (southeast - northwest direction as from areas $Q1 \leftrightarrow Q3$) directions respectively. The spatially specific mean $u_0(x)$ is modelled as having a quadratic form with an interaction term in the rotated grid. Letting $m(x)$ and $n(x)$ denote the relative ordering within the grid in either direction of location x (with $n(x), m(x) \in \{1, 2, \ldots, 13\}$ for a grid of size $13 \times 13 = 169$ as used in this study), it is assumed that

$$\begin{aligned}\mu_0(x) =& \mu_{0,1} + \mu_{0,2}m(x) + \mu_{0,3}n(x) + \mu_{0,4}m(x)^2 \\ &+ \mu_{0,5}n(x)^2 + \mu_{0,6}m(x)n(x)\end{aligned} \tag{4}$$

The spatio-temporal dynamic term $\theta(x,t)$ is modelled as a vector autoregressive model of order one, conditionally specified on its nearest neighbours in all cardinal directions, as shown in eq. (5).

$$\begin{aligned}\theta(x,t) =& b_0\theta(x,t-1) + b_N\theta(x^N,t-1) + b_E\theta(x^E,t-1) \\ &+ b_S\theta(x^S,t-1) + b_W\theta(x^W,t-1) + \varepsilon_\theta(x,t)\end{aligned} \tag{5}$$

The temporal component is modelled with a seasonal and a long-term trend part. The seasonal part is modelled as a combination of an annual and a semi-annual cyclic contribution (i.e. including the first two harmonic components) where the seasonal contribution is assumed invariant in space, as described by eq. (6).

$$M(t) = c\cos\omega t + d\sin\omega t + f\cos 2\omega t + g\sin 2\omega t + \varepsilon_m(t) \tag{6}$$

In order to include and isolate possible long-term effects of climate change in the model, the regression component on CO_2 concentrations in the atmosphere as described in eq. (7) has been included, assuming a combination of a linear and logarithmic relationship between the trend and the concentration level. It is noted that different alternatives for this components were investigated in Vanem et al. (2013), e.g. including a quadratic term and purely linear or logarithmic terms, and the linear-log form was found to be superior for the C-ERA-40 data. Hence, only this model alternative has been employed in this study, where the model is used to analyse the NORA10 data. In eq. (7) $G(t)$ denotes the average level of CO_2 in the atmosphere at time t (month). It is acknowledged that CO_2 is known to mix well in the atmosphere, so there is no spatial component in this regression term.

$$T(t) = \gamma G(t) + \eta G(t) + \varepsilon_T(t) \tag{7}$$

In the previous studies where the model was used to analyse the C-ERA-40 data, different model alternatives were tried out (Vanem 2012, 2013), but in this study, only the model according to eqs. (1) - (7) above has been utilized.

Prior distributions

In order to account for uncertainties in the model parameters, prior distributions are assigned to all model parameters and all inference and predictions are made on the posterior distribution. Hence, specifying prior distributions on all the model parameters, together with specification of initial values for $\theta(x,0)\ \forall x$, completes the specification of the model. In this study, prior distributions for all model parameters are assumed independent and conditionally conjugate priors will be specified for most priors to ensure that the conditional posterior distributions will be straightforward to derive. It is noted that the amount of data is quite large in this case and that therefore, the posteriors are not believed to be very sensitive to the exact values of the hyper-parameters; it is well known in Bayesian statistics that the posteriors are asymptotically independent of the priors as the amount of data increases. Similar priors as in the previous studies have been used, and details are not included in this paper.

Model implementation

Having completed the model specification and specified the priors, the derivation of the full conditionals for each model parameter is quite straightforward, as outlined in the appendix of Vanem (2013). Samples from the posteriors can then be obtained using MCMC methods, i.e. the Gibbs sampler with additional Metropolis-Hastings steps.

The MCMC methods for generating samples from the posterior distribution and hence inferring and making predictions from the model have been implemented in Java. Post-processing of the results, including preparation of plots, has been performed in **R**.

4. Simulation setup

As discussed above, five different subsets of the data have been investigated individually, in order to reduce the computation time; trying to run the model for the full dataset causes computations to become extremely time consuming and also increases the time for the MCMC chains to converge. Hence, the five subsets of (monthly maximum) data that have been analysed are (see Fig. 1):

- The complete area, but with every fourth data point in space (totalling 13 x 13 = 169 locations)
- Sub-area Q1 with every second data point in space (169 locations)
- Sub-area Q2 with every second data point in space (169 locations)
- Sub-area Q3 with every second data point in space (169 locations)
- Sub-area Q4 with every second data point in space (169 locations)

The MCMC simulations were run with a burn-in period of 40 000 samples and a batch size of 20. Hence, a total of 60 000 iterations were run to obtain a total of 1000 samples of the posterior parameter vector. In each iteration, the additional Metropolis-Hastings steps that were introduced to sample from the a_ϕ and a_λ parameters were repeated six times. This yields overall acceptance rates between 73% and 79% for the various simulation runs, which is more than sufficient to obtain good mixing properties of the chains.

Trace plots from the marginal sampled posterior distributions indicate stationarity and it is believed that the burn-in period is sufficient for the chain to converge. In the previous analyses of the C-ERA-40 data, some control runs were performed that indicated that burn-in periods far less than what has been employed in this study resulted in stationary chains and it is therefore assumed that convergence is likely also in the present study. However, the spatial fields are larger and might therefore need longer time to converge. Normal probability plots indicate that the Gaussian model assumption might be realistic.

With the settings above, simulations of the different sub-data sets with dimensions $169 \times 648 = 109\ 512$ data points complete well within a day.

5. Results and predictions

In this section, the results from the simulations of the different sub-sets of data will be presented. First, the results pertaining to the complete area, where every forth location was used will be presented. This can then be compared to the results for each of the four sub-areas that has been analysed with higher spatial resolution.

It is noted that the long-term trend contribution does not necessarily start at 0, so the estimated values of the time-independent contributions, $\mu(x)$, are adjusted to incorporate the mean value of the estimated trend component at year 2012 (see also the discussions in Vanem et al. (2013, 2012c)).

Complete area

The following results are from simulations run over the complete selected area, using every fourth grid-point in space.

The six parameters $\mu_{0,\cdot}$ determine the spatially varying mean $\mu_0(x)$ over the selected area. Together with the spatial dependence parameters a_ϕ and a_λ they determine the time independent spatial field $\mu(x)$. The estimated mean of this field for the complete selected area is illustrated in Fig. 7, where the x- and y-directions corresponds to the axes of the rotated grid with the NORA10 data. The results indicate that there are relatively small spatial variations over the area, with estimated values of the mean spatial field ranging from 7.5 to 7.8 meters over the area, with a mean value of 7.7 meters. This is less spatial variation than what was observed in the C-ERA-40 data, but since the NORA10 data covers a significantly smaller geographical area, this is reasonable.

For the space-time interaction component, the mean contribution from this term ranges from -2.1 to 1.4 meters over all locations and time points (except $t = 0$). The average contribution is close to zero as it should, and the

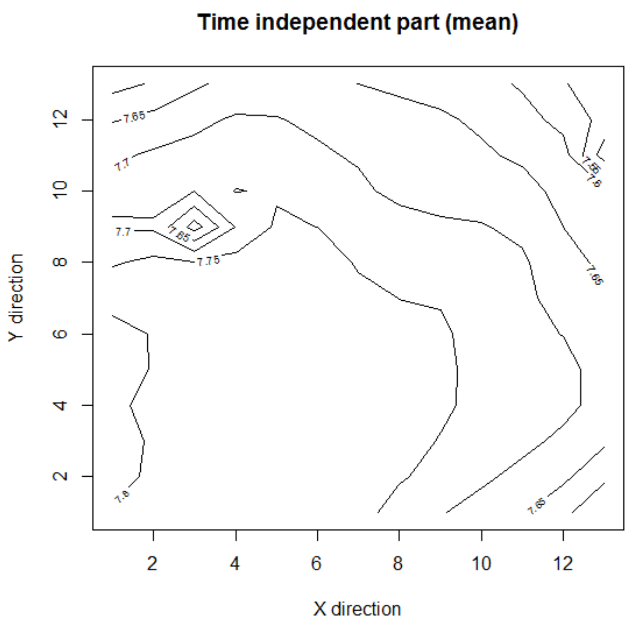

FIG. 7. The estimated spatial random field, $\mu(x)$, for the complete area

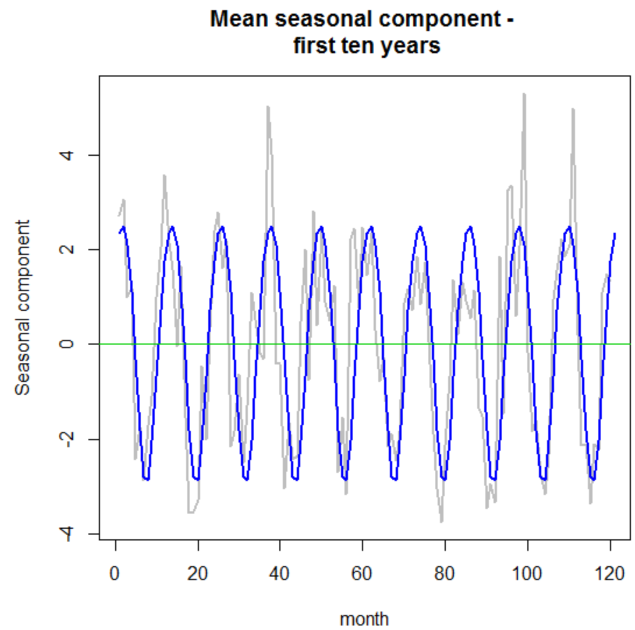

FIG. 8. The estimated seasonal contribution for the first ten years (complete area)

variances range from 0.047 to 0.37 m^2. This seems reasonable. Compared to the results for the C-ERA-40 data, it is observed that the range of contributions for the space-time dynamic part is of comparable order of magnitude, but with a slightly larger contribution from this term for the NORA10 data. This could possibly be explained by the higher spatial resolution of the NORA10 data, which might describe more of the short-term dynamics of the sea states. At any rate, the estimated values are deemed to be reasonable and a notable part of the modelled significant wave height can be ascribed to this component.

The estimated contribution from the seasonal component, $M(t)$, is shown in Fig. 8 for the first ten years, displaying a clear cyclic behaviour. The estimated seasonal contribution varies between -3.0 and 2.5 meters corresponding to a mean annual variation in the range of 5.5 meters for the monthly maximum data. This is comparable but slightly larger compared to the estimated seasonal variation in the C-ERA-40 data. The asymmetry between the seasonal minima and maxima is picked up by the model due to the inclusion of the second harmonic in the seasonal component, which is then warranted.

The estimated long-term trend over the period covered by the NORA10 data is illustrated in Fig. 9, including the mean and 90% credible intervals of the estimated trend. The trend contribution is adjusted so that it starts at zero. It is observed that the estimated trend signal is quite noisy, but that a mean increasing trend can be extracted. The estimated mean long-term trend over the data period is 21 cm, with a 90% credible interval ranging from -5.6 cm to 48 cm. Hence, even though the model extracts an increasing trend in the wave climate, this trend is not statistically significant at the 90% level. Compared to the trends extracted from the C-ERA-40 data (Vanem et al. 2013, 2012c), the trend estimated from the NORA10 data is slightly less. It is also noted that the trends estimated from C-ERA-40 data were statistically significant at the 90% level, whereas this ceases to be the case for the complete NORA10 data.

Assuming that the observed stochastic relationship between significant wave height and atmospheric levels of CO_2 remains unchanged in the future, future projections of significant wave height can be made based on different future emission scenarios. Projections obtained in this way by adopting the IPCC A2 and B1 scenarios, respectively, are illustrated in Fig. 10. With both scenarios, the mean future trend is increasing. It is observed that the extreme emission scenario A2 yields a higher expected future trend (note that the scales on the two figures are different), but that neither of the future trends are statistically significant at the 90% level. For the A2 emission scenario, the estimated mean accumulated trend between 2012 and 2100 corresponds to an increase of 1.4 meters, with 90% credible intervals ranging from a decrease of 1.2 m to an increase of 3.5 meters. The corresponding mean future in-

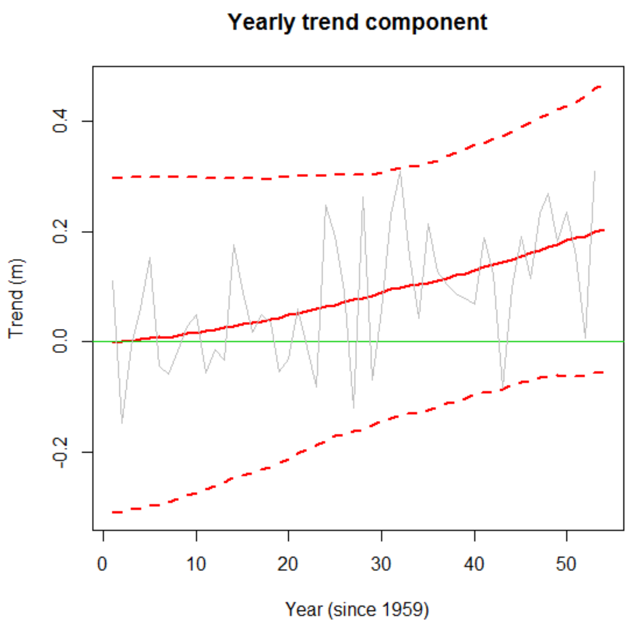

FIG. 9. Estimated long-term trend for the complete selected area

crease estimated by assuming the B1 emission scenario is 43 cm, with 90% credible intervals ranging from a decrease of 48 cm to an increase of 1.2 meters. Compared to the future projections made based on the C-ERA-40 data, this is considerable less. Nevertheless, the models identify an expected increase of the NORA10 ocean wave climate, albeit not statistically significant.

sub-areas

In addition to running the Bayesian hierarchical space-time on the complete selected area of NORA10 data, separate simulations have been run on four sub-areas, referred to as Q1 to Q4 (see Fig. 1). The setup of the simulations is identical to the simulations for the whole area and the results will be reported in the following. Since the sub-areas are obviously smaller in extension than the whole area, the spatial resolution has been doubled compared to the simulations for the whole area without increasing the computational time. Hence, the spatial grids are of the same size as before, but with shorter distances between grid points. A brief summary of the results for the various sub-areas is given below.

The estimated mean spatial fields are presented in Fig. 11 for all sub-areas. For the rest of the components, the figures are very similar to the ones for the complete area, and figures will not be presented. The ranges of estimated values for the different model components for each of the sub-areas are also included in Table 5. Also the estimated 90% credible intervals for the long term trends (1959 - 2012) and the future projections (2013 - 2100) are presented in Table 5.

6. Discussion and comparison of results

The simulations presented in the preceding sections use different sub-sets of data, which all stem from the same source, the NORA10. The differences are in spatial resolution and geographical location, with the four sub-areas essentially constituting the overall area.

The average spatial fields, $\mu(x)$, were estimated to be slightly different for the different simulations. It was just below 8 meters for the complete area, and varied slightly for the different sub-areas that were investigated. The smallest mean values were estimated for sub-area Q3, where the time-independent part varied from 6.3 - 6.6 m. For the other three sub-areas, the spatial fields were quite comparable with estimated mean values close to 8 meters. It is obviously not a problem that the average sea state conditions are slightly different for neighbouring geographical areas, but differences in the order of 1.5 m seem unrealistic. A possible explanation could be that the Markov chain for the spatial field for this particular area did not converge sufficiently. It is also noted that the estimated values of spatial fields for the different sub-areas were comparable to that estimated for the C-ERA-40 data. The spatial fields for the smaller sub-areas displayed slightly less spatial variability than for the overall area, but this could be expected since the geographical extent is smaller.

Also the estimated space-time interaction contribution, $\theta(x, t)$, is higher when applied to the whole area compared to either of the sub-areas with higher spatial resolution. For the whole area, the contribution from this component is a variability of 3.55 m, whereas the net contribution for the four sub-areas varies from 1.8 m (Q1) to 2.8 m (Q3). The explanation for this difference is not obvious, but since this component describes a short-term interaction between space and time, it should not be surprising that the contribution from this component is sensitive to the spatial resolution in the data. It is noted that for the C-ERA-40 data, this component was also found to be sensitive to the temporal resolution (Vanem et al. 2012a).

It is reassuring then to observe that the seasonal component behaves very similarly for all areas that have been investigated. The estimated expected seasonal variation is found to be 5.5 m for three of the sub-areas as well as the overall area. For the last sub-area, Q3, a slightly smaller seasonal variation of 5.3 m is estimated, which is still comparable. Hence, the results for the various sub-sets of the data are deemed to be consistent.

The perhaps most interesting contribution is the long-term trend that can possibly be related to climate change.

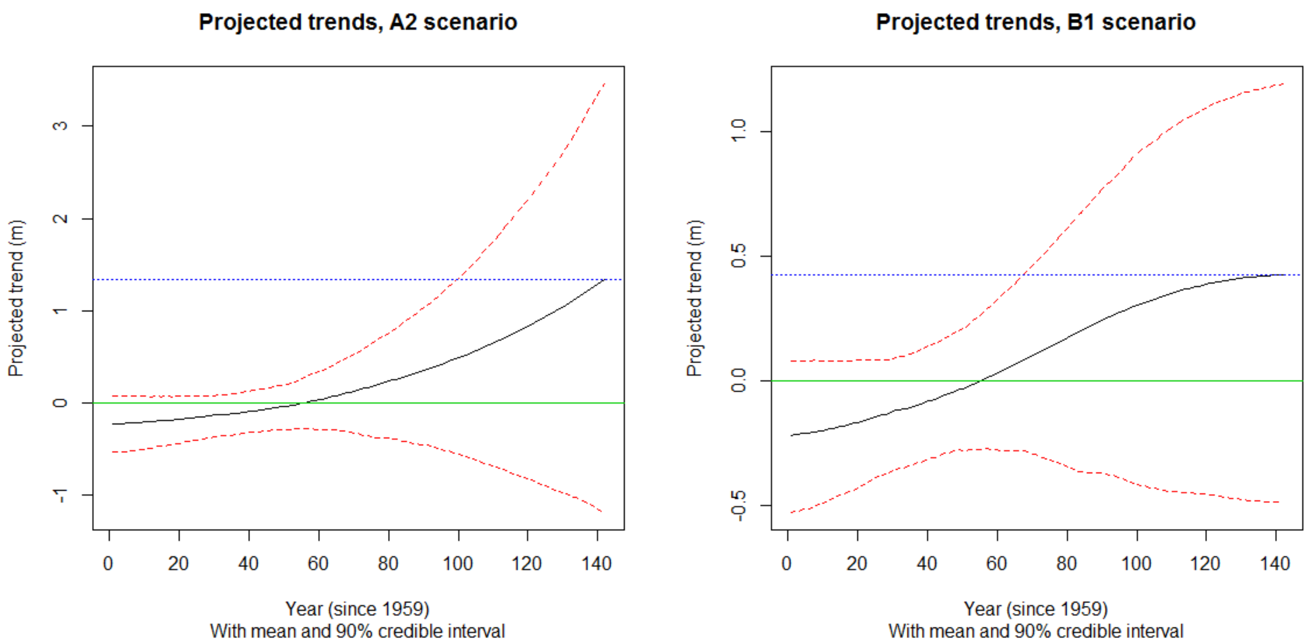

FIG. 10. Projected future trends in the significant wave height for the complete area

The estimated trend for the overall area is positive, but not significantly so at the 90% level. For the three first sub-areas investigated (Q1-Q3), the estimated mean long-term trends are still positive but smaller than the overall trend and still not significantly positive. However, for sub-area Q4, the estimated long term trend is found to be statistically significant and also slightly stronger than the trend estimated for the area overall. Notwithstanding the different estimates for the trend, the fact that the overall area has an estimated trend that falls between the other estimates suggests that the results are consistent. Moreover, the results indicate that there are large uncertainties as to whether there are any significant trends, but that the north-easterly corner of the overall area are expected to experience a stronger trend than the other parts of the area. The trends extracted by the Bayesian hierarchical space-time model are also consistent with the trend estimated by fitting a straight line by least squares. Estimated trends vary from 4 cm to 35 cm for the different sub-areas, with an estimated trend of 21 cm for the overall area, and this is believed to be consistent with the fitted straight line with an increase of about 29 cm for the spatial mean. Furthermore, the fact that most of the estimated trends are not statistically significant at the 90% level agrees with the results for the least square fitted linear trend (see Table 4).

The future projections are a result of the estimated long-term trends in the data. Hence, it is expected that future projections for sub-area Q4 are higher than for the other areas. This is indeed what is observed, but the uncertainties are large and the future projections for all areas fail to be statistically significant. Estimated mean future projections towards the year 2100 range from 27 cm (sub-area Q1) to 2.3 m (sub-area Q4) with an estimated expected increase of 1.9 m for the area overall, assuming emission scenario A2. For scenario B1, the corresponding range of mean estimates is 9 to 72 cm. These results are regarded as internally consistent, even though no statistically significant future projection of monthly maximum significant wave height is found.

Some control runs for three of the investigated areas were performed in order to see if increasing the burn-in would influence the results, i.e. for the overall area and for sub-areas Q3 and Q4. These control runs indicate that results for all but one of the model components are robust to changes in burn-in length, but that the spatial field estimates are sensitive to increased burn-in period. The spatial patterns of the estimated fields are similar but the estimated average levels are different for the initial and control runs. This is troublesome and indicates that the time-independent component fails to converge within the burn in period. Hence, the results for this particular component should not be trusted. This also raises the question of whether the other components area affected and to what extent. Obviously, all components in the model are interconnected, but it appears from the results that the other components are not very sensitive to the length of

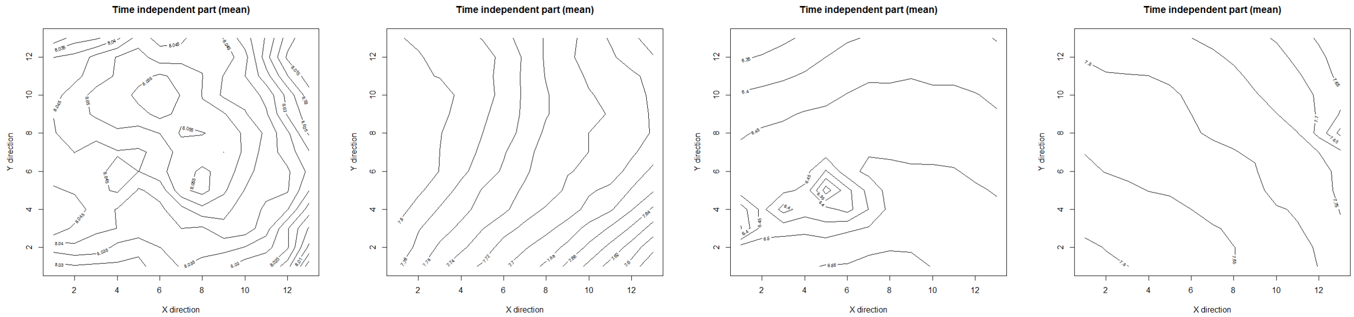

FIG. 11. The estimated mean spatial field for sub-areas Q1 (left)- Q4 (right)

TABLE 5. Range of estimated values for the different model components (m)

	Complete area	Q1	Q2	Q3	Q4
Spatial field	7.5 - 7.8	8.0 - 8.1	7.6 - 7.8	6.3 - 6.6	7.6 - 7.9
$\theta(x, t > 0)$	-2.1 - 1.4	-1.1 - 0.70	-0.72 - 0.81	-1.6 - 1.2	-0.95 - 0.97
Seasonal component	-3.0 - 2.5	-3.0 - 2.5	-3.0 - 2.5	-2.9 - 2.4	-3.0 - 2.5
Long-term trend	0.21	0.04	0.16	0.11	0.35
A2 projections	1.4	0.27	1.0	0.61	2.3
B1 projections	0.43	0.09	0.33	0.20	0.72
Trend: 90% c.i.	-0.056 - 0.48	-0.23 - 0.33	-0.14 - 0.54	-0.14 - 0.32	0.025 - 0.62
A2: 90% c.i.	-1.2 - 3.5	-2.5 - 3.2	-1.4 - 4.1	-2.5 - 3.2	-0.97 - 4.7
B1: 90% c.i.	-0.48 - 1.2	-0.95 - 1.1	-0.6 - 1.6	-0.97 - 1.2	-0.51 - 1.7

the burn in period. This might indicate that the convergence problems are isolated to the spatial field component, even though this cannot be assured. It is also unexpected that only the average level of the spatial field is difficult to estimate and that the model appears to be able to describe the spatial patterns of the fields consistently.

One explanation for the lack of convergence can be that the spatial field is quite large, and that it therefore takes time to explore the state space for the parameters obtained with the Metropolis-Hastings steps. These were drawn from a proposal distribution, and if the spatial field is large, the joint distribution might be very narrow leading to only small steps. However, the acceptance rate for the Metropolis-Hastings step is quite high in the simulations. Another explanation could be that the model is over-parametrised in the spatial component so that there are many solutions that lead to a reasonable fit. Still, it is unexpected that finding the mean level in the data should be difficult.

At any rate, it is observed that the results for all components except for the estimated average level of the spatial field are consistent and that the extended burn in period does not significantly alter these estimates. In particular, the results agree on an increasing, albeit not statistically significant, trend for all areas except the sub-area Q4 where the estimated trend is significantly increasing also for the control run.

Compared to the results for a similar analysis on the C-ERA-40 data, the NORA10 data display less significant long-term trends. In fact, whereas the models pick up a statistically significant increasing trend in the C-ERA-40 data, the identified trends in the NORA10 data are only statistically significant for one of the sub-areas that are investigated, i.e. Q4. This result is confirmed by the spatio-temporal model and was also found by fitting a straight line by least squares. One possible explanation for these results might be that the C-ERA-40 data previously investigated only covered the period until 2002, whereas the NORA10 data covers the period until 2012. A very crude investigation into the NORA10 data suggests that there is an increasing trend from 1958 until 2002 followed by a very slight decreasing trend from 2002 until 2012, for the spatial mean and spatial max time series. However, none of these trends are statistically significant. Furthermore, for the spatial min time series, the trend in the data is increasing throughout the period, although never being statistically significant.

It is also noted that the NORA10 data were obtained by downscaling of ERA-40 data and running a WAM model forced by ERA-40 wind fields, and it is therefore peculiar that the identified trends in the C-ERA-40 data for significant wave height disappear in the NORA10 data. However, when a similar analysis was performed on ERA-40 wind speeds, no particular long-term trends were picked up in the wind-speed data (Vanem and Breivik 2013).

7. Summary and conclusions

The Bayesian hierarchical space-time models for significant wave height that have previously been applied to C-ERA-40 data have been applied to NORA10 data for an overlapping area in the North-East Atlantic in this paper. Overall, the model seems to perform well in describing the temporal and spatial variations in the data, although the estimates pertaining to the average time-independent component are found to be sensitive to the length of the burn-in period.

Interestingly, the results from this analysis pertaining to long-term trends contradict previous results derived from C-ERA-40 data of significant wave height. Whereas the analysis of the C-ERA-40 data suggested that there are statistically significant increasing long-term trends over the area, the identified trends in the NORA10 data are not statistically significant (except for one of the quarter-areas investigated. Possible explanations to this could be that the geographical areas are not identical and that the NORA10 data covers 10 more recent years of data. However, similar results would be obtained if analysing NORA10 data up until 2002 only.

It is also noted that future projections made by the model are uncertain and even though an expected future increase in the monthly maximum significant wave height is estimated, the projections are uncertain with 90% credible intervals ranging from negative to positive trends.

Acknowledgments.

The work presented in this paper has been carried out with support from the Norwegian Research Concil (NRC) funded project ExWaCli.

Thanks to Ole Johan Årnes at the Norwegian Meteorological Institute, Bergen for kindly providing the NORA10 data used in the analysis, and to Profs. Bent Natvig and Arne Bang Huseby at University of Oslo for valuable discussions. Finally, thanks to Dr. Elzbieta Bitner-Gregersen at DNV R&I for valuable discussions and support.

REFERENCES

Aarnes, O. J., Ø. Breivik, and M. Reistad, 2012: Wave extremes in the northeast atlantic. *Journal of Climate*, **25**, 1529–1543.

Bitner-Gregersen, E. M., L. I. Eide, T. Hørte, and R. Skjong, 2012: *Ship and Offshore Structure Design in Climate Change perspective*. SpringerBrief in Climate Studies, Springer.

Breivik, Ø., O. J. Aarnes, J.-R. Bidlot, A. Carrasco, and Ø. Sætra, 2013: Wave extremes in the North East Atlantic from ensemble forecasts. *Journal of Climate*, **Early Online release**.

Caires, S. and V. Swail, 2004: Global wave climate trend and variability analysis. *Preprints of 8th International Workshop on Wave Hindcasting and Forecasting*.

DNV, 2010: Climate change and effect on marine structure design. Tech. rep., Det Norske Veritas. R&I Position Paper 1.

DNV, 2011: Potential impact of climate change on tanker design. Tech. rep., Det Norske Veritas. R&I Position Paper 8.

IPCC, 2001: *Climate Change 2001: The Scientific Basis*. Cambridge University Press.

Jain, A. K., H. S. Kheshgi, M. I. Hoffert, and D. J. Wuebbles, 1995: Distribution of radiocarbon as a test of global carbon cycle models. *Global Biogeochemical Cycles*, **9**, 153–166.

Komen, G., L. Cavaleri, M. Donelan, K. Hasselmann, S. Hasselmann, and P. Janssen, 1994: *Dynamics and Modelling of Ocean Waves*. Cambridge University Press.

Reistad, M., Ø. Breivik, and H. Haakenstad, 2007: A high-resolution hindcast study for the North Sea, the Norwegian Sea and the Barents Sea. *Preprints of 10th International Workshop on Wave Hindcasting and Forecasting and Coastal Hazards Symposium*.

Reistad, M., Ø. Breivik, H. Haakenstad, O. J. Aarnes, B. R. Furevik, and J.-R. Bidlot, 2011: A high-resolution hindcast of wind and waves for the North Sea, the Norwegian Sea and the Barents Sea. *Journal of Geophysical Research*, **116**, C05 019.

Sterl, A. and S. Caires, 2005: Climatology, variability and extrema of ocean waves: The web-based KNMI/ERA-40 wave atlas. *International Journal of Climatology*, **25**, 963–977.

Thoning, K. W., P. P. Tans, and W. D. Komhyr, 1989: Atmospheric carbon dioxide at Mauna Loa observatory 2. analysis of the NOAA GMCC data, 1974-1985. *Journal of Geophysical Research*, **94**, 8549–8565.

Undén, P., et al., 2002: *HIRLAM-5 Scientific Documentation*. SMHI, Sweden.

Vanem, E., 2012: Bayesian hierarchical space-time models for significant wave height data. Ph.D. thesis, University of Oslo.

Vanem, E., 2013: *Bayesian hierarchical spaec-time models with applications to significant wave height*. Ocean Engineering and Oceanography, Springer.

Vanem, E. and E. Bitner-Gregersen, 2012: Stochastic modelling of long-term trends in the wave climate and its potential impact on ship structural loads. *Applied Ocean Research*, **37**, 235–248.

Vanem, E. and O. N. Breivik, 2013: Bayesian hierarchical modelling of North Atlantic windiness. *Natural Hazards and Earth System Sciences*, **13**, 545–557.

Vanem, E., A. B. Huseby, and B. Natvig, 2011: A Bayesian-hierarchical space-time model for significant wave height data. *Proc. 30th International Conference on Offshore Mechanics and Arctic Engineering (OMAE 2011)*, American Society of Mechanical Engineers (ASME).

Vanem, E., A. B. Huseby, and B. Natvig, 2012a: A Bayesian hierarchical spatio-temporal model for significant wave height in the North Atlantic. *Stochastic Environmental Research and Risk Assessment*, **26**, 609–632.

Vanem, E., A. B. Huseby, and B. Natvig, 2012b: Modeling ocean wave climate with a Bayesian hierarchical space-time model and a log-transform of the data. *Ocean Dynamics*, **62**, 355–375.

Vanem, E., A. B. Huseby, and B. Natvig, 2013: Bayesian hierarchical spatio-temporal modelling of trends and future projections in the ocean wave climate with a CO_2 regression component. *Environmental and Ecological Statistics*, **in press**.

Vanem, E., B. Natvig, and A. B. Huseby, 2012c: Modelling the effect of climate change on the wave climate of the world's oceans. *Ocean Science Journal*, **47**, 123–145.

Vanem, E. and S.-E. Walker, 2012: Identifying trends in the ocean wave climate by time series analyses of significant wave height data. *Ocean Engineering*, **61**, 148–160.